ELSEVIER

J. Non-Newtonian Fluid Mech., 75 (1998) 77–97

Journal of Non-Newtonian Fluid Mechanics

On the stability of the simple shear flow of a Johnson–Segalman fluid

Georgios C. Georgiou [a,*], Dimitris Vlassopoulos [b]

[a] *Department of Mathematics and Statistics, University of Cyprus, PO Box 537, 1678 Nicosia, Cyprus*
[b] *Foundation for Research and Technology, Hellas (FORTH), Institute of Electronic Structure and Laser, PO Box 1527, Road to Voutes, 71110 Heraklion, Crete, Greece*

Received 24 May 1997

Abstract

We solve the time-dependent simple shear flow of a Johnson–Segalman fluid with added Newtonian viscosity. We focus on the case where the steady-state shear stress/shear rate curve is not monotonic. We show that, in addition to the standard smooth linear solution for the velocity, there exists, in a certain range of the velocity of the moving plate, an uncountable infinity of steady-state solutions in which the velocity is piecewise linear, the shear stress is constant and the other stress components are characterized by jump discontinuities. The stability of the steady-state solutions is investigated numerically. In agreement with linear stability analysis, it is shown that steady-state solutions are unstable only if the slope of a linear velocity segment is in the negative-slope regime of the shear stress/shear rate curve. The time-dependent solutions are always bounded and converge to a stable steady state. The number of the discontinuity points and the final value of the shear stress depend on the initial perturbation. No regimes of self-sustained oscillations have been found. © 1998 Elsevier Science B.V.

Keywords: Shear flow; Johnson–Segalman model; Stability

1. Introduction

Slip at the wall and constitutive instabilities are the main mechanisms proposed for explaining the instabilities observed during the extrusion of polymeric fluids from a capillary or a slit die [1–5]. The importance of slip is suggested by experiments carried out by various groups in the past 10 years. The slip mechanism has been proposed for explaining not only the stick-slip (or spurt or cyclic melt fracture) and gross melt fracture instabilities observed at high volumetric flow rates, but also the sharkskin instability observed at lower volumetric flow rates [1,6–8].

* Corresponding author. Tel.: +357 2 338701; fax: +357 2 339061; e-mail: georgios@pythagoras.mas.ucy.ac.cy

PII S0377-0257(97)00078-5

Based on the linear stability analysis of incompressible Newtonian Poiseuille flow with slip at the wall, Pearson [9] pointed out that the combination of a non-monotonic slip equation with melt compressibility can lead to self-sustained oscillations of the pressure drop and of the mass flow rate, similar to those observed experimentally with the stick-slip instability. Slip equations exhibiting non-monotonic behavior of the wall shear stress/velocity at the wall curve have been proposed by El Kissi and Piau [10], Leonov [11] and Hatzikiriakos and Dealy [7]. The non-monotone slip equation derived by Leonov [11], from a simple stochastic model of interface molecular dynamics for cross-linked elastomers, has recently been modified for polymer melts by Adewale and Leonov [5].

Georgiou and Crochet [12,13] verified the ideas of Pearson [9] by numerically solving the time-dependent compressible Newtonian Poiseuille and extrudate-swell flows with slip along the wall. Their calculations showed that steady-state solutions corresponding to the negative-slope regime of the slip equation are unstable in agreement with the linear stability analysis of Pearson and Petrie [14]. Compressibility acts as the storage of elastic energy that sustains the oscillations of the pressure drop and the mass flow rate and generates waves on the extrudate surface, in the case of the extrudate-swell problem.

The combination of compressibility and non-linear slip represents the underlying mechanism in various one-dimensional phenomenological models describing the oscillations of the pressure and the volumetric flow rate in the stick-slip instability regime (see [15] and references therein). These models require the calculation of certain parameters from experimental data and are based on the assumption that the time-dependent solution follows the hysteresis loop resulting from the non-monotonic flow curve. Moreover, the reservoir region is included and the compressibility of the fluid is taken into account.

The combination of non-linear slip and elasticity also leads to self-sustained oscillations, i.e. elasticity might replace compressibility and provide the elastic energy that sustains the oscillations. Georgiou [16] carried out a simple linear stability analysis of the simple shear flow of an Oldroyd-B fluid assuming that slip occurs along the fixed plate showing that steady-state solutions corresponding to the negative-slope regime of the slip equation might be unstable. The Oldroyd-B model was chosen because it exhibits a monotonic steady-shear response in the absence of slip. Numerical calculations for the time-dependent flow showed the existence of periodic solutions in the instability regime and that the amplitude and period of the oscillations are increasing functions of the elasticity. Similar results have been obtained by Brasseur et al. [17], who solved numerically the one- and two-dimensional Poiseuille flows of an Oldroyd-B fluid with slip along the wall. The two-dimensional calculations revealed the existence of a second mode of periodicity in space and that the amplitude and the period of the oscillations are smaller than in the one-dimensional case.

Whereas the mechanism of slip-induced instability is based on the multi-validness of the slip equation, constitutive instabilities are caused by the multi-valuedness of the constitutive equation. The non-monotonicity of the shear stress as a function of shear rate can physically be thought of as a separation of flow into two dynamic regimes, one with a history of high deformation rate (near the boundary) and one with a history of low deformation rate (away from the boundary) [18]. This, in turn, implies that two characteristic times of the viscoelastic fluid, a short and a long one, are relevant. The physical interpretation is that the Rouse relaxation time controls chain conformation at short times or high rates (local rod motions),

whereas reptation-like times control the motion of chains at larger scale [19]. Based on this concept, the association of non-monotonic constitutive equations with two relaxation times to the spurt effect observed in well-defined experiments has been recently established [19,20].

Multivalued constitutive equations seem to appropriate for wormlike surfactant semidilute solutions, which exhibit a narrow spectrum of relaxation times [21]. The flow birefringence experiments of Decruppe et al. with a CTAB solution in circular Couette flow showed that the flow is divided into two layers when the apparent shear rate exceeds a critical value [22]. Mair and Callaghan have also carried out Couette flow experiments with a different surfactant solution and used nuclear magnetic resonance to image both velocity and diffusion [21]; they observed apparent slip at the inner wall as well as a high shear rate band located away from the wall in the body of the fluid, i.e. they discerned at least three bands.

It should be emphasized that the use of the constitutive instability mechanism for explaining the spurt instability for polymer melts or solutions has been criticized by some investigators. Adewale and Leonov have shown that the Johnson–Segalman model is unable to match simultaneously the experimental data for narrow-distributed polyethylene in the critical regime of shear flow leading to the spurt phenomenon and in the critical regime of elongational flow [23] and underline the fact that non-monotone flow curves have been reported only for some materials with yield stress and not for common polymer melts or elastomers [5]. They also point out that the upper branch of the apparent flow curve is strongly dependent on the capillary radius and it is doubtful whether this dependence can be explained without slip [5]. The experimental results of Piau et al. [24] and Wang and Drda [4] support the interfacial nature of the stick-slip transition which is found to depend on the surface roughness and the surface energy of the capillary die. Larson also notes that, indeed, the main drawback of the constitutive instability approach is that it cannot account for diameter effects [2]. On the other hand, Aarts and van de Ven [25] note that the critical volumetric flow rate for the Johnson–Segalman fluid does scale with the radius, and this is consistent with the experimental data of El Kissi and Piau [26]. It is possible that both wall slip and constitutive instability are present, since there is physical significance to both [2]. Interesting discussions about the two mechanisms of instability can be found in [27,5]. Finally, in order to explain the whole range of extrusion instabilities, additional important factors must be taken into account, such as viscous heating [28], fracture of the melt in the die entry region and free energy for creating a new surface [5].

Linear stability and/or time-dependent numerical analyses of the shear and Poiseuille flows of the three-constant Oldroyd model [29], the Doi–Edwards model with a Rouse relaxation mode [18,30], the Johnson–Segalman model with an added Newtonian viscosity [31–35] and the Giesekus model with the value of the anisotropy coefficient greater than 1/2 [31,36,37] show that steady-state solutions in the negative-slope regime of the constitutive equation may be unstable and that a flow curve hysteresis is obtained between the two positive-slope stable branches, in pressure controlled loading and unloading experiments.

A consequence of the non-monotonicity of the constitutive models is that, in one-dimensional flows, such as the simple shear and Poiseuille flows, they allow multiple steady-state solutions in a certain range of the shear rate. In addition to the standard steady-state solution, there exist uncountable infinite weak solutions which are characterized by an arbitrary number of shear rate discontinuities. In Poiseuille flow, these discontinuities are located in the vicinity of the wall where the shear rate can be high. The narrow high shear rate layer near the wall leads to an

apparent slip, whereas the flow in the bulk might be almost plug. The appearance of zones of different shear rates is also referred to as shear banding [21].

Kolkka et al. [31] considered the simple shear and plane Poiseuille flows of a Johnson–Segalman fluid with an added Newtonian viscosity and showed that piecewise smooth solutions with local shear rate corresponding to the descending portion of the steady shear stress/shear rate curve are linearly unstable. Their numerical calculations for pressure gradient-controlled Poiseuille flow showed that the time-dependent solution jumps to one of the two stable positive-slope branches of the steady shear stress/shear rate curve and thus the negative-slope branch is unattainable. On the other hand, Malkus et al. [34] obtained numerical time-dependent results for the startup of Poiseuille flow i.e. at fixed volumetric flow rate. For certain values of the material parameters, the calculated pressure drop appeared to be oscillatory but, as the authors pointed out, the existence of a true oscillatory regime was not certain due to the difficulty in accurately distinguishing slightly damped systems in numerical calculations. Denn remarked that the oscillations obtained by Malkus et al. [34] are not of the type of the slip induced persistent oscillations between the two stable branches of the flow curve that are observed experimentally with polydisperse LLDPE in the stick-slip instability regime [1]. The existence of a 'true' oscillatory regime has been recently established for Poiseuille flows and has been corroborated by Aarts and van de Ven [25] and Kolkka and Ma [38]; it has been demonstrated that there is a Hopf bifurcation from an unstable steady-state [38].

More recently, Español et al. solved the two-dimensional plane shear flow of a Johnson–Segalman fluid with added Newtonian viscosity using a Lagrangian Eulerian method and taking the Reynolds number to be zero [35]. They also presented analytical and one-dimensional calculations for the zero Reynolds number case. Their shear flow inception results strongly suggest that, when the nominal shear rate is in the negative slope region of the constitutive equation, there is only one discontinuity point in the final steady state and that there exists a selection mechanism for the position of the discontinuity. In other words, they found that the flow is separated into two layers with the lower shear rate one being adjacent to the fixed wall. However, their numerical method is unable to capture the shear rate discontinuity. They use averagings in both space and time and their interface is not sharp, extending over eight of the 50 layers into which their domain is decomposed. Español et al. also found that there is a selection mechanism of the steady total shear stress, the value of which is roughly constant for all nominal shear rates in the negative slope region of the constitutive equation [35]. Greco and Ball solved numerically the circular Couette flow of a Johnson–Segalman fluid at zero Reynolds number and reported a similar selection mechanism for the final shear stress at the interfaces of the bands into which the flow is separated [39]. They obtained results with two and three bands at low and high velocities of the rotating cylinder, respectively. The appearance of three bands seems to agree with available experimental data [21].

In this paper, we consider the simple shear flow of a Johnson–Segalman fluid with added Newtonian viscosity. Our objective is to study numerically the stability of the piecewise linear steady-state solutions and investigate the dynamics of the flow for different initial conditions. The governing equations and the boundary conditions for the time-dependent flow problem are presented in Section 2. The steady-state solutions are given in Section 3. It is shown that, in addition to the standard linear solution for the velocity, there exists an uncountable infinity of piecewise linear steady-state solutions, in a certain range of the velocity of the moving plate.

Analytical time-dependent solutions for the limiting case of inertialess flow are also derived. In Section 4, the time-dependent flow is numerically solved and the stability of the steady-state solutions is investigated. For the viscoelastic part of the stress tensor, we use discontinuous finite element approximations, in order to avoid the appearance of Gibbs-type oscillations in the numerical solution. For the time integration, we employ the standard fully-implicit scheme. In accordance with the linear stability findings of Kolkka et al. [31], steady-state solutions are unstable only if the slope of a linear velocity segment is in the negative-slope regime of the shear stress/shear rate curve. However, the number of the stable steady-state solutions is infinite. The time-dependent solutions are always bounded and converge to a stable steady-state solution as time goes to infinity. The size of the perturbation, determines which steady-state solution will be attained. Oscillatory time-dependent solutions are observed in certain cases but the oscillations always decay with time, in contrast to the numerical results of Malkus et al. [34] for plane Poiseuille flow. Our numerical results for the inception of simple shear flow at zero Reynolds number disagree with those reported by Español et al. [35]. No selection mechanisms have been observed for the position of the discontinuity point and the final value of the total shear stress; in fact, our calculations show that the number of discontinuities can be more than one. Our conclusions are summarized in Section 5.

2. Governing equations

We consider the time-dependent simple shear (Couette) flow of a Johnson–Segalman fluid with added Newtonian viscosity. It is convenient to decompose the extra stress tensor $\boldsymbol{T}$ into a purely viscoelastic component $\boldsymbol{T}_1$ and a purely viscous component $\boldsymbol{T}_2$ (see, for example, [40]):

$$\boldsymbol{T} = \boldsymbol{T_1} + \boldsymbol{T_2}, \tag{1}$$

$$\boldsymbol{T_1} + \lambda \overset{\square}{\boldsymbol{T}}_{\boldsymbol{1}} = 2\eta_1 \boldsymbol{d}, \tag{2}$$

$$\boldsymbol{T_2} = 2\eta_2 \boldsymbol{d}, \tag{3}$$

where $\boldsymbol{d}$ is the rate-of-deformation tensor defined by

$$\boldsymbol{d} = \frac{1}{2}[(\nabla \boldsymbol{v}) + (\nabla \boldsymbol{v})^T], \tag{4}$$

$\boldsymbol{v}$ is the velocity vector, $\nabla \boldsymbol{v}$ is the velocity gradient tensor, λ is the relaxation time, and η_1 and η_2 have dimensions of viscosity. The sum $\eta_1 + \eta_2$ is the zero shear viscosity and the ratio $\eta_2/(\eta_1 + \eta_2)$ represents the ratio of the retardation time to the relaxation time. The derivative $\overset{\square}{\boldsymbol{T}}_{\boldsymbol{1}}$ is a linear combination of the upper- and lower-convected derivatives of $\boldsymbol{T}_1$, $\overset{\triangledown}{\boldsymbol{T}}_{\boldsymbol{1}}$ and $\overset{\triangle}{\boldsymbol{T}}_{\boldsymbol{1}}$, respectively:

$$\overset{\square}{\boldsymbol{T}}_{\boldsymbol{1}} = \left(1 - \frac{\xi}{2}\right) \overset{\triangledown}{\boldsymbol{T}}_{\boldsymbol{1}} + \frac{\xi}{2} \overset{\triangle}{\boldsymbol{T}}_{\boldsymbol{1}}, \tag{5}$$

where

$$\overset{\nabla}{\boldsymbol{T}}_1 = \frac{\partial \boldsymbol{T}_1}{\partial t} - (\nabla \boldsymbol{v})^{\mathrm{T}} \cdot \boldsymbol{T}_1 - \boldsymbol{T}_1 \cdot \nabla \boldsymbol{v}, \tag{6}$$

$$\overset{\triangle}{\boldsymbol{T}}_1 = \frac{\partial \boldsymbol{T}_1}{\partial t} + \nabla \boldsymbol{v} \cdot \boldsymbol{T}_1 + \boldsymbol{T}_1 \cdot (\nabla \boldsymbol{v})^{T}, \tag{7}$$

where $\partial \boldsymbol{T}_1/\partial t$ is the substantial time derivative of $\boldsymbol{T}_1$, the superscript T denotes the transpose of a tensor and ξ is a dimensionless material (slip) parameter varying from 0 to 2. The physical meaning of ξ, as suggested by Gordon and Schowalter [41], is that the corresponding stress and deformation convected derivatives relate to a non-affine motion, which actually characterizes the motion of a polymer strand end-to-end vector with respect to the macroscopic motion of the continuum; in such a case, the strand can slip by transmitting only a fraction of its stress to the continuum. Hence, ξ can be viewed as a measure of the contribution of non-affine motion to the shear tensor. For $\xi = 0$, the motion is affine and the model is reduced to the Oldroyd-B model. For $\xi = 2$, the motion is completely non-affine and the Oldroyd–Jaumann model is recovered. The upper-convected Maxwell model is recovered for $\xi = 0$ and $\eta_2 = 0$.

We would like at this point to proceed using dimensionless equations. We scale the length by the distance between the two plates H, the velocity by a characteristic velocity V^*, the stress components by $(\eta_1 + \eta_2)V^*/H$, and the time by H/V^*. This scaling leads to two dimensionless numbers, the Reynolds number, Re, and the Weissenberg number, We:

$$\mathrm{Re} \equiv \frac{\rho V^* H}{\eta_1 + \eta_2}, \tag{8}$$

$$\mathrm{We} \equiv \frac{\lambda V^*}{H}, \tag{9}$$

where ρ is the constant density.

The geometry and the boundary conditions of the plane shear flow are shown in Fig. 1. The fluid is placed between two parallel infinite plates located at $y = 0$ and 1. The lower plate moves with constant imposed velocity V, whereas the upper plate is fixed. The problem is one-dimensional [$\partial \cdot/\partial x = 0$, $v_x = v_x(y, t)$, $v_y = 0$ and $\boldsymbol{T}_1 = \boldsymbol{T}_1(y, t)$] and the continuity equation is automatically satisfied. The x-momentum equation is reduced to:

$$\mathrm{Re}\,\frac{\partial v_x}{\partial t} = \frac{\partial T_1^{xy}}{\partial y} + \frac{\partial T_2^{xy}}{\partial y} = \frac{\partial \mathrm{T}_1^{xy}}{\partial y} + \eta_2 \frac{\partial^2 v_x}{\partial y^2}. \tag{10}$$

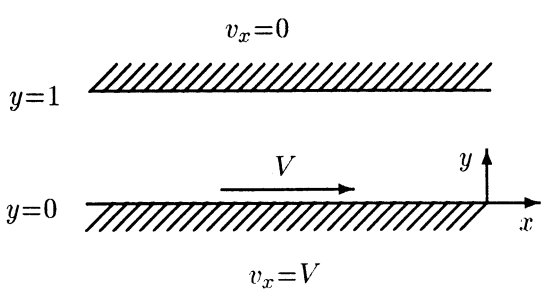

Fig. 1. Boundary conditions for the time-dependent simple shear flow.

For the components of $\mathbf{T_1}$, one gets:

$$T_1^{xx} + \mathrm{We}\,\frac{\partial T_1^{xx}}{\partial t} = 2\mathrm{We}\left(1-\frac{\xi}{2}\right)\frac{\partial v_x}{\partial y}\,T_1^{xy}; \tag{11}$$

$$T_1^{xy} + \mathrm{We}\,\frac{\partial T_1^{xy}}{\partial t} = \eta_1\,\frac{\partial v_x}{\partial y} + \mathrm{We}\,\frac{\partial v_x}{\partial y}\left[\left(1-\frac{\xi}{2}\right)T_1^{yy} - \frac{\xi}{2}\,T_1^{xx}\right]; \tag{12}$$

$$T_1^{yy} + \mathrm{We}\,\frac{\partial T_1^{yy}}{\partial t} = -\mathrm{We}\xi\,\frac{\partial v_x}{\partial y}\,T_1^{xy}. \tag{13}$$

All the variables in the above two equations are dimensionless, including η_1 and η_2 which are scaled by the zero shear viscosity; the dimensionless zero shear viscosity, $\eta_1+\eta_2$, is thus equal to unity.

3. Analytical solutions

In this section, we provide the steady-state solutions of the system of Eqs. (10)–(13) and obtain analytical time-dependent solutions for the limiting case of zero Re.

3.1. Steady-state solutions

In steady state, Eq. (10) gives

$$T^{xy} = T_1^{xy} + \eta_2\,\frac{\partial v_x}{\partial y} = T_1^{xy} - \eta_2\,\dot\gamma = \text{const.}, \tag{14}$$

where $\dot\gamma = -\partial v_x/\partial y$ is the shear rate. From Eqs. (11)–(14), one then gets

$$T_1^{xy} = -\frac{\eta_1\dot\gamma}{1+2\xi\left(1-\frac{\xi}{2}\right)(\mathrm{We}\dot\gamma)^2} \tag{15}$$

and

$$T_{xy} = -\left[\eta_2 + \frac{\eta_1}{1+2\xi\left(1-\frac{\xi}{2}\right)(\mathrm{We}\dot\gamma)^2}\right]\dot\gamma = \text{const.} \tag{16}$$

$$T^{xx} = T_1^{xx} = \frac{2\left(1-\frac{\xi}{2}\right)\eta_1\mathrm{We}\dot\gamma^2}{1+2\xi\left(1-\frac{\xi}{2}\right)(\mathrm{We}\dot\gamma)^2} \tag{17}$$

$$T^{yy} = T_1^{yy} = -\frac{\xi\eta_1\mathrm{We}\dot\gamma^2}{1+2\xi\left(1-\frac{\xi}{2}\right)(\mathrm{We}\dot\gamma)^2}. \tag{18}$$

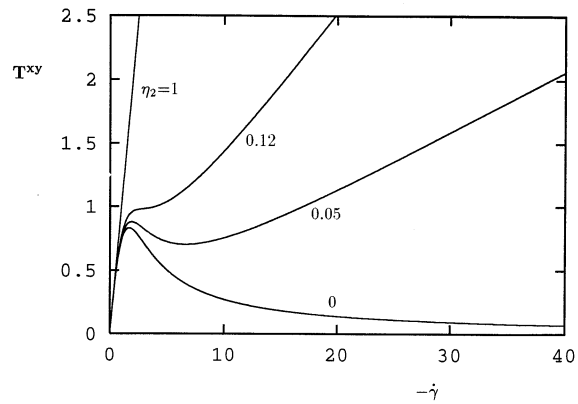

Fig. 2. Steady-state shear stress/shear rate curves for We = 1, $\xi = 0.2$ and different values of η_2. The curves for $\eta_2 = 0.05$ and 0 are calculated assuming that v_x is linear.

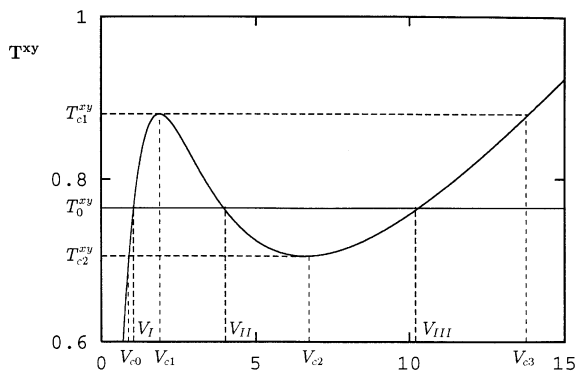

Fig. 3. Steady-state shear stress/shear rate curve for $\eta_2 = 0.05$, We = 1 and $\xi = 0.2$; definition of various symbols.

In Fig. 2, the shear stress T^{xy} is plotted as a function of the shear rate $\dot{\gamma}$ for different values of η_2, ranging from 0 up to 1. For $\eta_2 > 1/9$, T^{xy} is an increasing function of the shear rate. In such a case, to a given value of T^{xy} there exists only one value of $\dot{\gamma}$ or, equivalently, only one value of the velocity V of the lower plate, and the velocity v_x is linear:

$$v_x = (y-1)\dot{\gamma} = (1-y)V. \tag{19}$$

If, however, $\eta_2 < 1/9$, Eq. (16) exhibits a local maximum which is followed by a minimum, except if $\eta_2 = 0$ (Fig. 2). In such a case, there is a range of the shear stress T^{xy} in which three values of $\dot{\gamma}$ (or V) are possible. Of course, one solution for v_x is the smooth one given by Eq. (19) which is unstable according to the linear stability analysis of Kolkka et al. [31]. What is most interesting, however, is the existence of an uncountable infinity of solutions not following Eq. (19). Due to the multivaluedness of the constitutive equation, the velocity v_x can be piecewise linear with an arbitrary number of shear rate discontinuities; for a given value of the velocity V of the lower plate, there exist solutions at different values of the shear stress. Some of these solutions will be constructed below for We = 1, $\eta_2 = 0.05$ and $\xi = 0.2$. As easily seen

from Eqs. (17) and (18), for the latter value of ξ the ratio of the second to the first normal stress difference is 0.1.

Let (V_{c1}, T^{xy}_{c1}) and (V_{c2}, T^{xy}_{c2}) be the maximum and minimum points of Eq. (16), $V_{c0} < V_{c1}$ be the value of V at which $T^{xy}(V_{c0}) = T^{xy}(V_{c2}) = T^{xy}_{c2}$ and $V_{c3} > V_{c2}$ be the value of V at which $T^{xy}(V_{c3}) = T^{xy}(V_{c1}) = T^{xy}_{c1}$. The steady-state solution is not unique when the velocity of the moving plate $V \in (V_{c0}, V_{c3})$. We will first construct solutions consisting of two linear segments, choosing any value T^{xy}_0 of the shear stress in the interval $(T^{xy}_{c2}, T^{xy}_{c1})$ (the case $T^{xy}_0 = T^{xy}(V)$ is not excluded). To the chosen value T^{xy}_0 there correspond three velocities V_{I}, V_{II} and V_{III} with $V_{\mathrm{I}} < V_{\mathrm{II}} < V_{\mathrm{III}}$, as shown in Fig. 3. Let us assume that the slopes of the two linear segments of v_x are $-V_{\mathrm{I}}$ and $-V_{\mathrm{III}}$:

$$v_x = \begin{cases} V - V_{\mathrm{I}} y, & \text{if } 0 \le y \le y^*, \\ V + (y^* - y) V_{\mathrm{III}} - y^* V_{\mathrm{I}}, & \text{if } y^* \le y \le 1, \end{cases} \tag{20}$$

where $y^* \in (0, 1)$. The value of y^* is determined by demanding that v_x be zero at $y = 1$:

$$y^* = \frac{V_{\mathrm{III}} - V}{V_{\mathrm{III}} - V_{\mathrm{I}}}. \tag{21}$$

It is obvious that Eq. (16) is satisfied, since

$$T^{xy}(V_{\mathrm{I}}) = T^{xy}(V_{\mathrm{III}}) = T^{xy}_0. \tag{22}$$

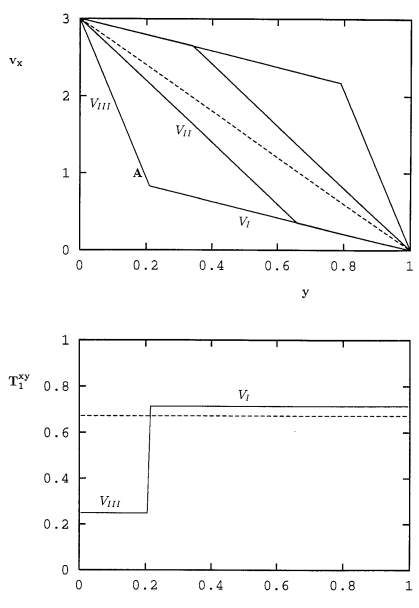

Fig. 4. (a) Steady-state solutions for v_x with one discontinuity point and corresponding to the same value of the shear stress. Solutions with a segment of slope V_{II} are unstable. (b) The component T^{xy}_1 corresponding to profile A of Fig. 4a. The broken lines show the standard smooth solution. We = 1, $\eta_2 = 0.05$, $\xi = 0.2$ and $V = 3$.

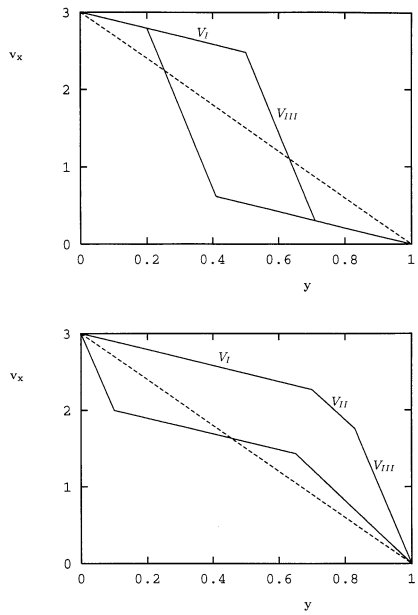

Fig. 5. (a) Two of the infinite stable steady-state solutions for v_x consisting of three linear segments of slope V_{I} and V_{II} and corresponding to the same value of the shear stress. (b) Two of the infinite unstable steady-state solutions for v_x consisting of three linear segments of slope V_{I}, V_{II} and V_{III}. The broken lines show the standard smooth solution. We $= 1$, $\eta_2 = 0.05$, $\xi = 0.2$ and $V = 3$.

It is also easy to see that another solution corresponding to V and T_0^{xy} and consisting of two linear segments is the following:

$$v_x = \begin{cases} V - V_{\mathrm{III}} y, & \text{if } 0 \le y \le y^*, \\ V + (y^* - y)V_{\mathrm{I}} - y^* V_{\mathrm{III}}, & \text{if } y^* \le y \le 1, \end{cases} \tag{23}$$

where now

$$y^* = \frac{V - V_{\mathrm{I}}}{V_{\mathrm{III}} - V_{\mathrm{I}}}. \tag{24}$$

The two velocity profiles given by Eqs. (20) and (23) are not the only two-segment solutions corresponding to the shear stress T_0^{xy}. There are another two solutions with segments of slope $-V_{\mathrm{I}}$ and $-V_{\mathrm{II}}$ if $V \in (V_{\mathrm{I}}, V_{\mathrm{II}})$ or of slope $-V_{\mathrm{II}}$ and $-V_{\mathrm{III}}$ if $V \in (V_{\mathrm{II}}, V_{\mathrm{III}})$. In Fig. 4a, we show all four two-segment solutions for v_x corresponding to the same shear stress value T_0^{xy}.

As predicted by the linear stability analysis of Kolkka et al. [31] and observed in the numerical calculations of the present work, steady-state solutions with a segment of slope $-V_{\mathrm{II}}$ (corresponding to the negative-slope regime of Eq. (16)) are unstable. Therefore, two steady-state solutions of Fig. 4a are unstable. Other solutions consisting of two linear segments can be constructed for any other value of T^{xy} in the interval $(T_{c2}^{xy}, T_{c1}^{xy})$. It should be noted that the shear rate and the components of $\boldsymbol{T}_1$ are discontinuous at the points where the slope of v_x changes. In Fig. 4b, we plot the component T_1^{xy} corresponding to one of the velocities of Fig. 4a. The behavior of T_1^{xx} and T_1^{yy} is similar.

Solutions consisting of three or more segments can also be constructed. Even in the rather simple case in which we have three linear segments of slope $-V_{\mathrm{I}}$, $-V_{\mathrm{III}}$ and $-V_{\mathrm{I}}$, there is an infinite number of solutions for a given value of T_0^{xy}. One can actually choose the position of one of the two discontinuity points. Two such solutions are plotted in Fig. 5a. Finally, in Fig. 5b, we show solutions with three segments of different slope ($-V_{\mathrm{I}}$, $-V_{\mathrm{II}}$ and $-V_{\mathrm{III}}$). As already mentioned, these solutions are unstable to small perturbations, since they contain a segment of slope $-V_{\mathrm{II}}$.

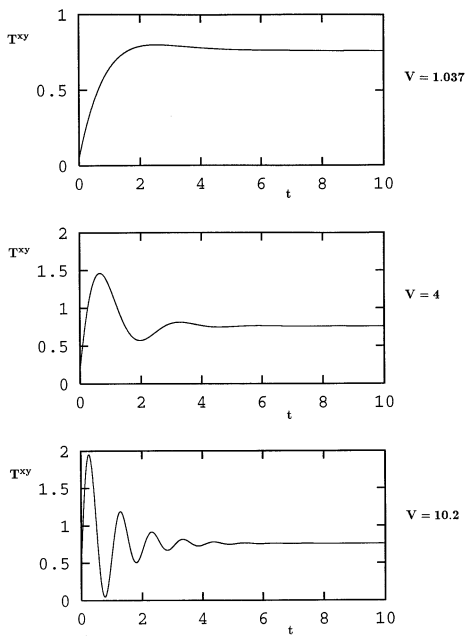

Fig. 6. Growth of T^{xy} during the inception of simple shear flow for zero Re, We = 1 and various values of V. It is assumed that a linear velocity profile is instantaneously attained. $\eta_2 = 0.05$ and $\xi = 0.2$.

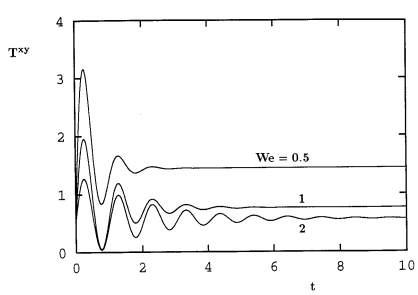

Fig. 7. Growth of T^{xy} during the inception of simple shear flow for zero Re, $V = 10.2$ and various values of We. It is assumed that a linear velocity profile is instantaneously attained. $\eta_2 = 0.05$ and $\xi = 0.2$.

3.2. Time-dependent results for $Re = 0$

By introducing the first normal stress difference

$$N_1 = T_1^{xx} - T_1^{yy}, \tag{25}$$

and the new stress variable

$$Z = \frac{\xi}{2} T_1^{xx} + \left(1 - \frac{\xi}{2}\right) T_1^{yy},$$

Eqs. (11)–(13) can be written as follows:

$$N_1 + \mathrm{We} \frac{\partial N_1}{\partial t} = 2\mathrm{We} \frac{\partial v_x}{\partial y} T_1^{xy}; \tag{27}$$

$$T_1^{xy} + \mathrm{We} \frac{\partial T_1^{xy}}{\partial t} = \eta_1 \frac{\partial v_x}{\partial y} + \mathrm{We} \frac{\partial v_x}{\partial y}\left[- \xi\left(1 - \frac{\xi}{2}\right) N_1 + (1 - \xi) Z \right]; \tag{28}$$

$$Z + \mathrm{We} \frac{\partial Z}{\partial t} = 0. \tag{29}$$

From Eq. (29), one observes that Z exhibits a trivial exponential decay; it will always be zero, provided that it is zero at $t = 0$. Under this assumption, the number of unknown fields is reduced by one. In the limiting case of inertialess flow ($\mathrm{Re} = 0$), the x-momentum equation gives

$$T_1^{xy} + \eta_2 \frac{\partial v_x}{\partial y} = T^{xy}(t),$$

i.e. the shear stress T^{xy} is independent of the spatial coordinate y. We now assume that v_x attains one of the steady-state solutions at $t = 0$ (this is obvious if the fluid is Newtonian). In such a case, for a given linear segment of v_x of slope $\dot{\gamma}_{Ni}$, the corresponding viscoelastic shear stress T_{1i}^{xy} is independent of the spatial coordinate y. Combining Eqs. (27) and (28) leads to the following ODE:

$$(\mathrm{We})^2 \frac{\mathrm{d}^2 T_{1i}^{xy}}{\mathrm{d}t^2} + 2\mathrm{We} \frac{\mathrm{d}T_{1i}^{xy}}{\mathrm{d}t} + \left[1 + 2\xi\left(1 - \frac{\xi}{2}\right)(\mathrm{We}\dot{\gamma}_{Ni})^2\right] T_{1i}^{xy} = \eta_1 \dot{\gamma}_{Ni}. \tag{31}$$

The solution of Eq. (31) is

$$T_{1i}^{xy} = T_{1Ni}^{xy} + (T_{10}^{xy} - T_{1Ni}^{xy}) e^{-\frac{t}{\mathrm{We}}} (\cos \omega t - \mathrm{We}\, s\omega \sin \omega t), \tag{32}$$

where

$$\omega = \sqrt{2\xi\left(1 - \frac{\xi}{2}\right)}\dot{\gamma}_{Ni} \tag{33}$$

T_{10}^{xy} is the viscoelastic shear stress at $t = 0$ and T_{1Ni}^{xy} is the steady-state value of T_1^{xy} corresponding to the shear rate $\dot{\gamma}_{Ni}$. Obviously, the shear stress is damped oscillatorily towards a steady-state solution with a frequency given by Eq. (33).

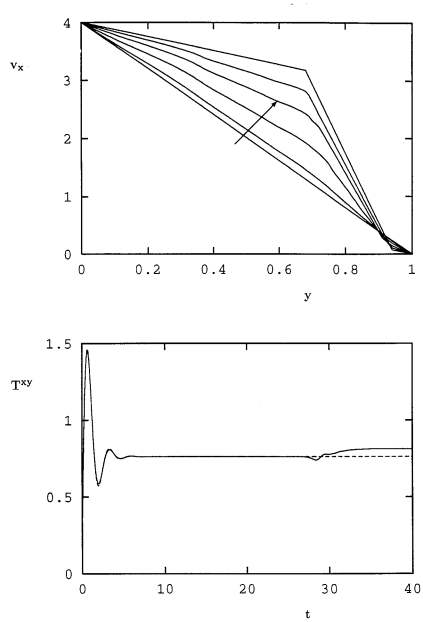

Fig. 8. Transition from an unstable smooth steady state to a stable discontinuous one. Inception of simple shear flow for zero Re, $V=4$, We $=1$, $\eta_2=0.05$ and $\xi=0.2$: (a) velocity; (b) shear stress at the upper plate. The dashed line is a prediction of Eq. (32).

Let us consider the inception of simple shear flow. The fluid is initially at rest and all the stress components are zero at $t=0$. We assume that the lower plate moves with a constant velocity V at all times after $t=0$ and that v_x instantaneously becomes linear. The shear stress growth predicted by Eq. (32) for We $=1$ and various values of V is shown in Fig. 6. For small shear rates i.e. for small values of V, the shear stress approaches the steady-state value monotonically. Decaying oscillations appear at higher shear rates, in agreement with experimental observations [42]. Note that the standard (linear) steady-state solution for $V=4$ is linearly unstable, since it corresponds to the negative slope regime of the shear stress/shear rate curve and practically it cannot be reached. The numerical simulations in Section 4 show that any perturbation, independently of its size, will lead to one of the infinite stable solutions with discontinuous shear stress and piecewise linear velocity. In Fig. 7, the shear stress growth for $V=10.2$ and various values of We is shown. The decay of the oscillations becomes slower and their wavelength decreases with elasticity.

4. Numerical results

To discretize Eqs. (10)–(13) in space, we use mixed finite elements and the Galerkin method. An important issue is the compatibility of the approximations used for the two unknown fields, v_x and $\boldsymbol{T}_1$. Another complication, however, arises from the fact that the unknown components of $\boldsymbol{T}_1$ are discontinuous (except when v_x is linear). Using continuous approximations (i.e. linear

or biquadratic) for these unknowns leads to Gibbs-type oscillations of the numerical solution. Therefore, we have used zeroth-order approximations for $\boldsymbol{T}_1$ (i.e. its components are taken constant over each element). For the velocity v_x we have used a biquadratic (P^2-C^0) approximation. Most of the results presented here have been obtained with 100 elements. The convergence of the solution has been checked, however, using 200 and 500 elements. For the integration in time, we use the standard fully-implicit (Euler backward difference) scheme. As for the initial condition, we start from a steady-state solution obtained for a given velocity V_0 of the lower plate and at time $t=0$ we set its velocity equal to the desired value V. In all the subsequent results, the time step Δt is taken equal to 0.001, $\mathrm{We}=1$, $\eta_2=0.05$ and $\xi=0.2$.

In order to test the numerical code, we first studied the limiting case of zero Reynolds number and made comparisons with the analytical time-dependent solutions of Section 3.2. We calculated the inception of simple shear flow for various values of V. In general, the numerical results agree with the analytical solution: the velocity v_x becomes linear at the first time step and the shear stress T_{xy} is independent of y and follows Eq. (32). If the linear solution is unstable, however, i.e. if $V_{c1}<V<V_{c2}$, even a small rounding error suffices for the destabilization of the solution initiating the transition to a stable discontinuous solution. This is illustrated in Fig. 8, where we show results for $V=4$, obtained using 100 elements. In Fig. 8a, we plot velocity profiles calculated at different times and in Fig. 8b, we plot the calculated value of the shear stress at the lower plate as a function of time. Up to $t=26$, the velocity is linear and the shear stress is independent of y, in agreement with the predictions of Eq. (32). The solution then starts evolving to a stable steady-state solution with two discontinuity points at a higher shear stress. Reducing the mesh size or decreasing the time step leads to other stable steady-state solutions

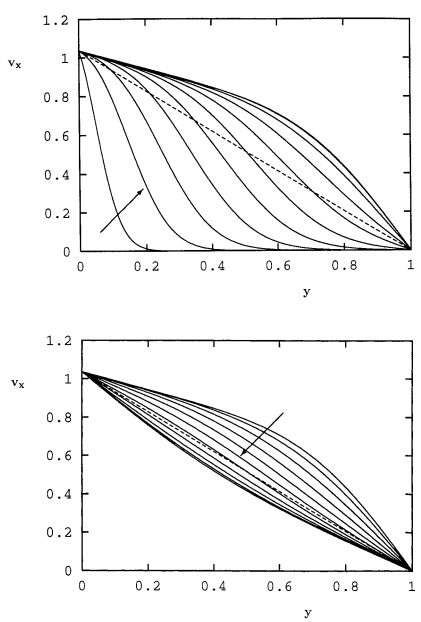

Fig. 9. Evolution of v_x during the inception of simple shear flow for $V=1.037$, $\mathrm{Re}=1$, $\mathrm{We}=1$, $\eta_2=0.05$ and $\xi=0.2$: (a) times up to 1.05; (b) times from 1.05 to 2.05. The dashed line is the final steady-state.

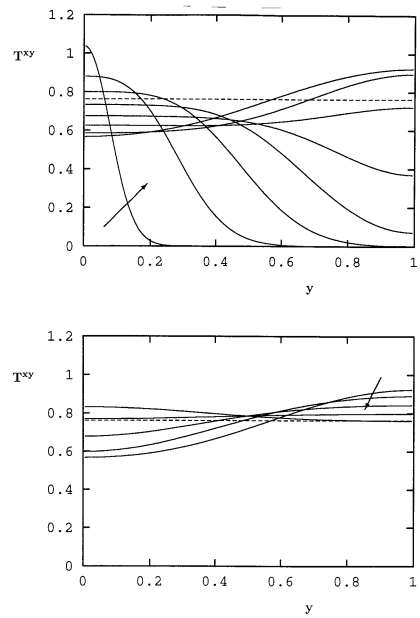

Fig. 10. Evolution of T^{xy} during the inception of simple shear flow for $V = 1.037$, $\mathrm{Re} = 1$, $\mathrm{We} = 1$, $\eta_2 = 0.05$ and $\xi = 0.2$: (a) times up to 1.45; (b) times from 1.45 to 2.25. The dashed line is the final steady-state.

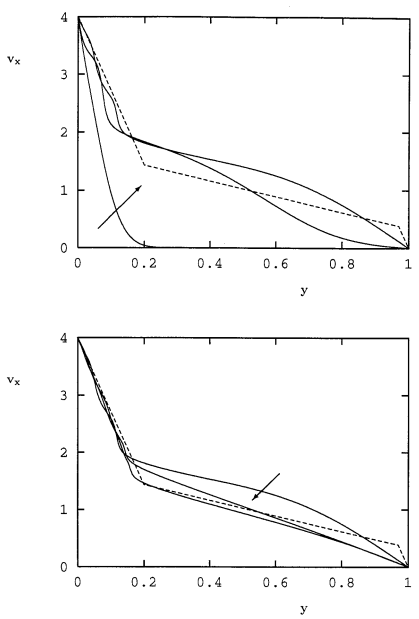

Fig. 11. Evolution of v_x during the inception of simple shear flow for $V = 4$, $\mathrm{Re} = 1$, $\mathrm{We} = 1$, $\eta_2 = 0.05$ and $\xi = 0.2$: (a) times up to 1.05; (b) times from 1.05 to 2.25. The dashed line is the final steady-state.

with more discontinuity points at different shear stress values, since the numerical perturbation is different. Therefore, the initial perturbation determines which stable steady state will be attained. Our results thus disagree with those of Español et al. [35] who found that there is only one discontinuity point in the final steady-state solution and that there exists a selection mechanism for the value of the final total shear stress. For a given nominal shear rate, one can actually choose the value of the final shear stress and the number of discontinuity points and construct a stable velocity profile at $t = 0$. The components of $\boldsymbol{T}_1$ in each layer will then follow the analytical solution Eq. (31). As a final remark, the numerical results for zero Reynolds number exhibit the latency phenomenon which is observed in pressure gradient controlled Poiseuille flows for non-monotonic constitutive equations. Similar results were obtained by Ganpule [43].

We now move to the non-zero Reynolds number case and set $\mathrm{Re} = 1$. We calculated the inception of simple shear flow for various values of V in all different regimes of the standard shear stress/shear rate curve: (a) $V = 1.037 \in (V_{c0}, V_{c1})$, the evolutions of v_x and T^{xy} are shown in Figs. 9 and 10, respectively; (b) $V = 4 \in (V_{c1}, V_{c2})$, the evolution of v_x is shown in Fig. 11; (c) $V = 10.2 \in (V_{c2}, V_{c3})$, the evolution of v_x is illustrated in Fig. 12a. The shear stress at the upper plate is plotted in Fig. 12b as a function of time; (d) $V = 20 \in (V_{c3}, \infty)$, the evolution of v_x is shown in Fig. 13a and the shear stress at the upper plate is plotted in Fig. 13b. Note that the first three velocities are in the interval (V_{c0}, V_{c3}) in which there exist multiple steady-state solutions. The same results have been obtained using a more refined mesh and a smaller time step. The results can be summarized as follows: (i) if $V \in (V_{c0}, V_{c1}) \cup (V_{c2}, V_{c3})$, v_x evolves to one stable steady-state which might be either smooth (e.g. $V = 1.037$ in Fig. 9) or discontinuous (e.g.

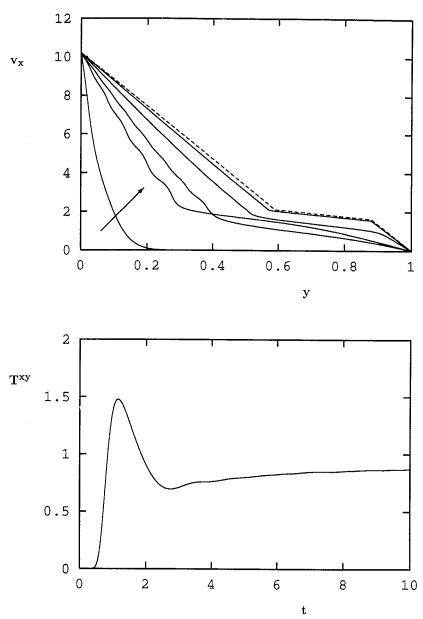

Fig. 12. Inception of simple shear flow for $V = 10.2$, $\mathrm{Re} = 1$, $\mathrm{We} = 1$, $\eta_2 = 0.05$ and $\xi = 0.2$: (a) evolution of v_x; the dashed line is the final steady-state; (b) evolution of the shear stress at the upper plate.

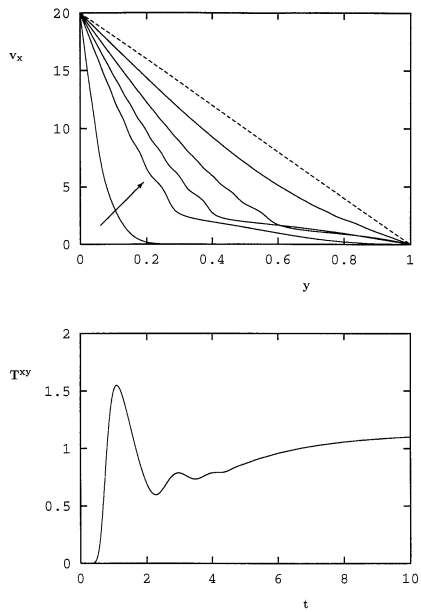

Fig. 13. Inception of simple shear flow for $V = 20$, $\mathrm{Re} = 1$, $\mathrm{We} = 1$, $\eta_2 = 0.05$ and $\xi = 0.2$: (a) evolution of v_x; the dashed line is the final steady-state; (b) evolution of the shear stress at the upper plate.

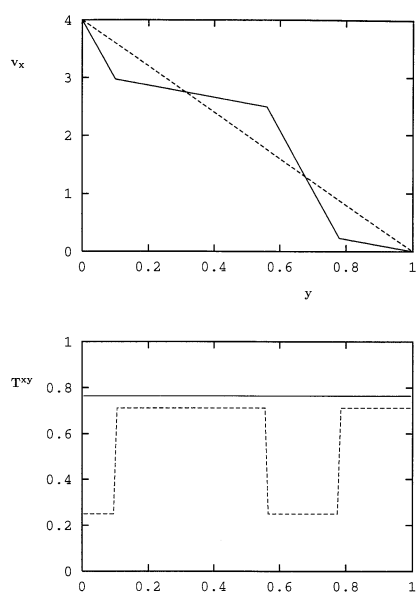

Fig. 14. One of the stable discontinuous steady-state solutions obtained for $V = 4$, $\mathrm{Re} = 1$, $\mathrm{We} = 1$, $\eta_2 = 0.05$, $\xi = 0.2$ and $V_0 = 3.9$: (a) velocity v_x; the dashed line is the unstable smooth steady state; (b) shear stress T_i^{xy}; the dashed line is T_1^{xy}.

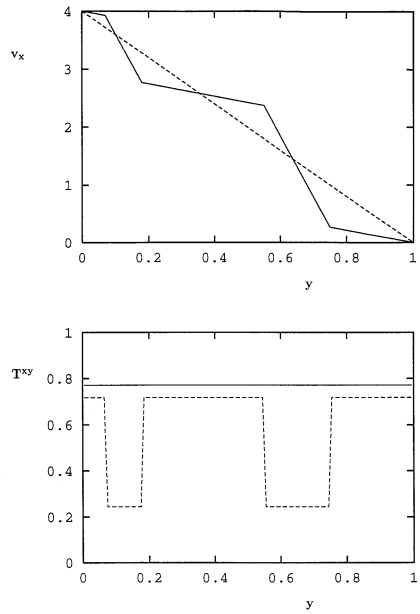

Fig. 15. Another stable discontinuous steady-state solution obtained for $V=4$, $\mathrm{Re}=1$, $\mathrm{We}=1$, $\eta_2=0.05$, $\xi=0.2$ and $V_0=4.000001$: (a) velocity v_x; the dashed line is the unstable smooth steady state; (b) shear stress T_i^{xy}; the dashed line is T_1^{xy} .

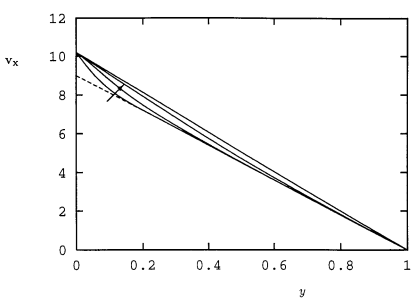

Fig. 16. Evolution of v_x for $V=10.2$ starting from the linear solution for $V_0=9$ (dashed line); $\mathrm{Re}=1$, $\mathrm{We}=1$, $\eta_2=0.05$ and $\xi=0.2$.

$V=10.2$ in Fig. 12); (ii) if $V\in(V_{c1}, V_{c2})$, the linear steady-state solution is unstable and thus only discontinuous solutions can be attained (e.g. $V=4$ in Fig. 11); (iii) if $V\in(0, V_{c0})\cup(V_{c3}, \infty)$, the unique stable linear solution is reached (e.g. $V=20$ in Fig. 13).

As already mentioned, the initial perturbation determines which one of the infinite stable steady states will be reached in the case $V\in(V_{c0}, V_{c3})$. In Figs. 14 and 15a, we show two of the final velocity profiles obtained for $V=4$ starting from $V_0=3.9$ and 4.000001, respectively. In Fig. 14b and 15b, the corresponding final profiles of T^{xy} and T_1^{xy} are depicted. Solutions with more discontinuity points can more easily be obtained by slightly perturbing an unstable discontinuous steady-state or even by sufficiently perturbing a stable discontinuous steady state.

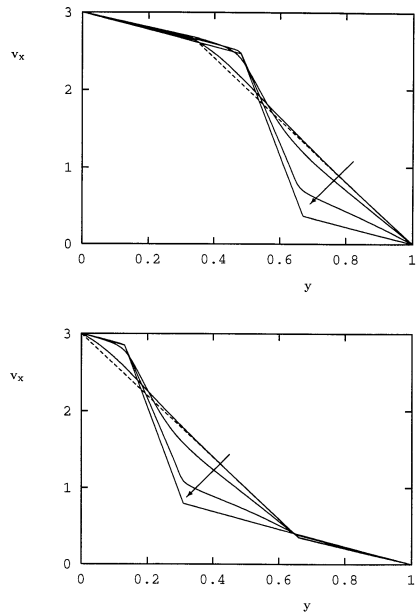

Fig. 17. Evolution of v_x after slightly perturbing the two unstable steady-state solutions of Fig. 4a ($V = 3$). Dashed lines show the unstable solution. $\mathrm{Re} = 1$, $\mathrm{We} = 1$, $\eta_2 = 0.05$ and $\xi = 0.2$.

In Fig. 16, we show the evolution of v_x for $V = 10.2$ calculated for $V_0 = 9$. The perturbation is small compared to that of the start up flow ($V_0 = 0$, Fig. 12) and the stable linear solution is obtained in this case. Finally, in Fig. 17, we show two examples of transition from an unstable discontinuous solution to a stable one. The two unstable two-segment solutions of Fig. 4a for $V_0 = 3$ have been perturbed by setting $V = 3.01$. The final steady states contain two discontinuity points in both cases.

Numerical calculations have also been carried out for other values of the material parameters. In all cases, the time dependent solutions are bounded and converge to a stable steady state as $t \to \infty$. At high shear rates some oscillations are observed initially but they decay with time (Fig. 12b and 13b). No regimes of periodic solutions, similar to those reported by Malkus et al. [34] for plane Poiseuille flow, have been detected. It should be pointed out that oscillations observed in the special case of $\eta_2 = 0$ or for small values of η_2 are not real. The system of Eqs. (13)–(19) is ill-posed in such a case, since the second-order derivative term of Eq. (10) vanishes and yet two boundary conditions for v_x need to be satisfied.

5. Conclusions

The stability of the discontinuous steady-state solutions of the simple shear flow of a Johnson–Segalman fluid with an added Newtonian viscosity has been investigated by means of finite element calculations. The numerical results show that piecewise smooth solutions are unstable if they contain segments in which the local shear rate corresponds to the negative-slope

branch of the steady shear stress/shear rate curve, in agreement with the linear stability results of Kolkka et al. [31]. The time-dependent solutions are bounded and converge to different stable steady-state solutions, depending on the initial perturbation. Our results for the inception of simple shear flow at zero Reynolds number seem to be in disagreement with those of Español et al. [35] and Greco and Ball [39]. The number of discontinuity points in the final steady-state solution can be more than one and the final value of total shear stress is not the same for all nominal shear rates in the unstable regime of the constitutive equation. In contrast to the numerical results of Malkus et al. [34] for plane Poiseuille flow, time periodic solutions are not obtained in any range of the material parameters. Thus, the fact that non-monotonic constitutive equations allow the existence of unstable steady states in some range of the shear rate cannot alone be used for explaining the stick-slip instability.

Acknowledgements

Part of this research was supported by the European Community (Brite/Euram Program, Grant BRE2-CT94.0610). GG is grateful to all the members of the Polymer Group of the I.E.S.L. (FORTH) for their warm hospitality during his 4 month stay in Heraklion.

References

[1] M.M. Denn, Ann. Rev. Fluid Mech. 22 (1990) 13–34.
[2] R.G. Larson, Rheol. Acta 31 (1992) 213–263.
[3] R.G. Larson, in: A. Aït-Kadi, J.M. Dealy, D.F. James, M.C. Williams (Eds.), Proceedings of the 12th International Congress of Rheology, Chemical Engineering Department, Laval University, Quebec, 1996, pp. 115–118.
[4] S.-Q. Wang, P.A. Drda, Rheol. Acta 36 (1997) 128–134.
[5] K.E.P. Adewale, A.I. Leonov, Rheol. Acta 36 (1997) 110–127.
[6] J.M. Piau, N. El Kissi, B. Tremblay, J. Non-Newtonian Fluid Mech. 34 (1990) 145–180.
[7] S.G. Hatzikiriakos, J.M. Dealy, J. Rheol. 36 (1992) 703–741.
[8] S.-Q. Wang, P.A. Drda, Y.-W. Inn, J. Rheol. 40 (1996) 875–898.
[9] J.R.A. Pearson, Mechanics of Polymer Processing, Elsevier, London, 1985.
[10] N. El Kissi, J.M. Piau, C. R. Acad. Sci. Ser. II 309 (1989) 7–9.
[11] A.I. Leonov, Wear 141 (1990) 137–145.
[12] G.C. Georgiou, M.J. Crochet, J. Rheol. 38 (1994) 639–654.
[13] G.C. Georgiou, M.J. Crochet, J. Rheol. 38 (1994) 1745–1755.
[14] J.R.A. Pearson, C.J.S. Petrie, in: Proceedings of the 4th International Congress on Rheology, vol. 3, 1965, pp. 265–282.
[15] V. Durand, B. Vergnes, J.F. Agassant, E. Benoit, R.J. Koopmans, J. Rheol. 40 (1996) 383–394.
[16] G.C. Georgiou, Rheol. Acta 35 (1996) 39–47.
[17] E. Brasseur, G.C. Georgiou, V. Navez, M.J. Crochet, Symposium on Rheology and Computational Fluid Mechanics, Nicosia, Cyprus, July 4–5, 1996.
[18] T.C.B. McLeish, R.C. Ball, J. Polym. Sci. B24 (1986) 1735–1745.
[19] J.A. Deiber, W.R. Schowalter, J. Non-Newtonian Fluid Mech. 40 (1991) 141–150.
[20] D. Vlassopoulos, S.G. Hatzikiriakos, J. Non-Newtonian Fluid Mech. 57 (1995) 119–136.
[21] R.W. Mair, P.T. Callaghan, J. Rheol. 41 (1997) 901–924.
[22] J.P. Decruppe, R. Cressely, R. Makhloufi, E. Cappelaere, Colloid Polym. Sci. 273 (1995) 346–351.

[23] K.E.P. Adewale, A.I. Leonov, J. Non-Newtonian Fluid Mech. 49 (1993) 133–138.
[24] J.M. Piau, N. El Kissi, F. Toussaint, A. Mezghani, Rheol. Acta 34 (1995) 40–57.
[25] K. Aarts, A.A.F. van de Ven, in: H. Neurzert (Ed.), Progress in Industrial Mathematics at EMCI94, Wiley, Chichester, 1996, pp. 216–223.
[26] N. El Kissi, J.-M. Piau, J. Non-Newtonian Fluid Mech. 37 (1990) 55–94.
[27] Y.-L. Chen, R.G. Larson, S.S. Patel, Rheol. Acta 33 (1994) 243–256.
[28] E.E. Rosenbaum, S.G. Hatzikiriakos, AIChE J. 43 (1997) 598–608.
[29] J. Yerushalmi, S. Katz, R. Shinnar, Chem. Eng. Sci. 25 (1970) 1891–1902.
[30] T.C.B. McLeish, J. Polym. Sci. B25 (1987) 2253–2264.
[31] R.W. Kolkka, D.S. Malkus, M.G. Hansen, G.R. Ierley, R.A. Worthing, J. Non-Newtonian Fluid Mech. 29 (1988) 303–335.
[32] J.A. Nohel, R.L. Pego, A.E. Tzavaras, Proc. R. Soc. Edinburgh A115 (1990) 39–59.
[33] D.S. Malkus, J.A. Nohel, B.J. Plohr, SIAM J. Appl. Math. 51 (1991) 899–929.
[34] D.S. Malkus, J.A. Nohel, B.J. Plohr, in: J.F. Dijksman, G.D. Kuiken (Eds.), Numerical Simulation of Non-Isothermal Flow of Viscoelastic Liquids, Kluwer, Dordrecht, 1993, pp. 57–71.
[35] P. Español, X.F. Yuan, R.C. Ball, J. Non-Newtonian Fluid Mech. 65 (1996) 93–109.
[36] R. Kolkka, G. Ierley, J. Non-Newtonian Fluid Mech. 33 (1989) 305–323.
[37] D.S. Malkus, J.A. Nohel, B.J. Plohr, J. Comput. Phys. 87 (1990) 464–487.
[38] R.W. Kolkka, Private communication, 1997.
[39] F. Greco, R.C. Ball, J. Non-Newtonian Fluid Mech. 69 (1997) 195–206.
[40] M.J. Crochet, A.R. Davies, K. Walters, Numerical Simulation of Non-Newtonian Flow, Elsevier, Amsterdam, 1984.
[41] R.J. Gordon, W.R. Schowalter, Trans. Soc. Rheol. 16 (1972) 79–97.
[42] R.B. Bird, R.C. Armstrong, O. Hassager, Dynamics of Polymeric Liquids, Wiley, New York, 1987.
[43] T. Ganpule, A constitutive analysis of anomalous shear flows for highly entangled nearly monodisperse polymer melts and solutions, M.Sc. Thesis, Michigan Technological University, 1992.

.